Dissecting FcγR Regulation Through a Multivalent Binding Model

Ryan A. Robinett[a], Ning Guan[a], Anja Lux[b], Markus Biburger[b], Falk Nimmerjahn[b], **Aaron S. Meyer[c]**

[a]Koch Institute for Integrative Cancer Research, Massachusetts Institute of Technology, Cambridge, MA; Contributed equally
[b]Friedrich-Alexander-University of Erlangen-Nürnberg
[c]Department of Bioengineering, Jonsson Comprehensive Cancer Center, Eli and Edythe Broad Center of Regenerative Medicine and Stem Cell Research; University of California, Los Angeles

https://asmlab.org

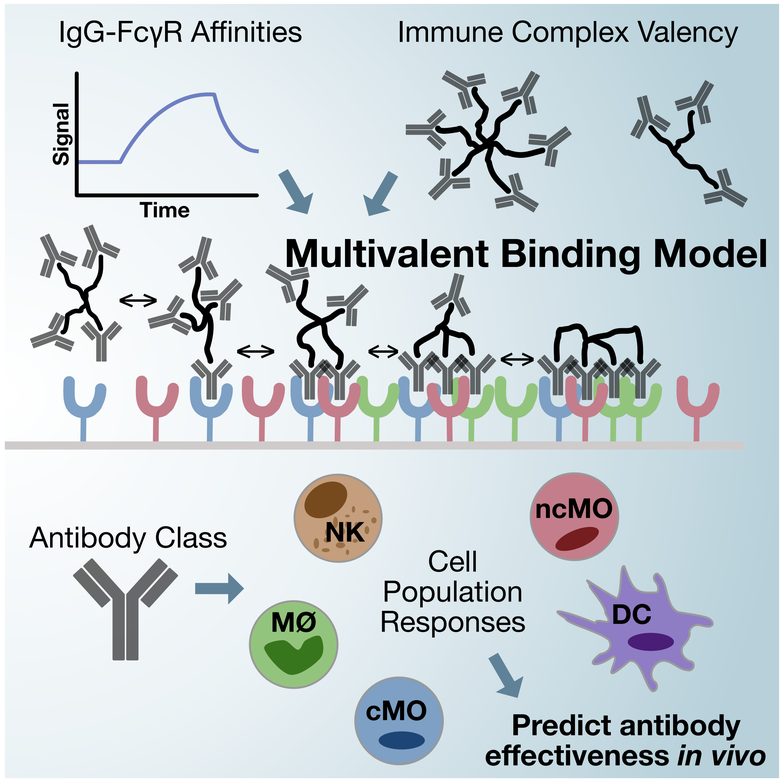

IgG-FcγR binding varies with affinity and valency

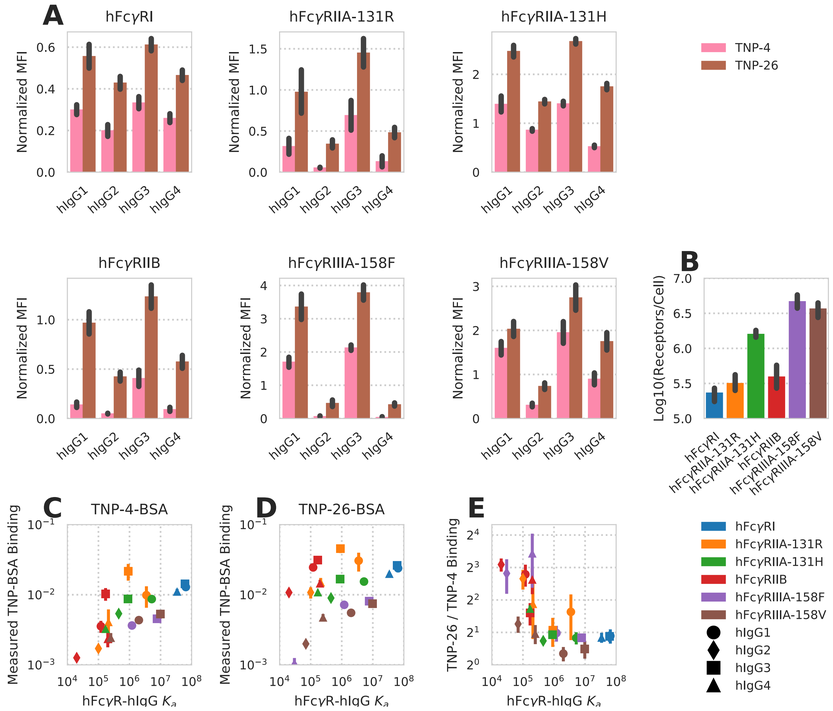

Figure 1: Human FcγR binding changes with FcγR-IgG pair and valency. **A)** Quantification of hIgG subclass TNP-4-BSA and TNP-26-BSA IC binding to CHO cells expressing the indicated hFcγRs (N = 4). Background binding of the ICs to CHO cells expressing no hFcγR was subtracted from the mean fluorescence intensity (MFI) obtained from binding to CHO cells expressing individual hFcγRs. Each IC binding measurement was further normalized by dividing by the average of all the points within that replicate. **B)** Receptor expression quantification for each CHO cell line expressing a single hFcγR subclass. **C-D)** Measured TNP-4-BSA-IC (C) and TNP-26-BSA-IC (D) binding, normalized to the receptor expression within each CHO cell line, as a function of the measured hFcγR-hIgG subclass affinity. **E)** Fold increase in TNP-26-BSA binding over TNP-4-BSA binding as a function of the measured hFcγR-hIgG subclass affinity. All error bars are standard error of biological replicates (N = 4). Derived quantities use error propagated from each value.

A multivalent interaction model accounts for variation in FcγR-IgG binding

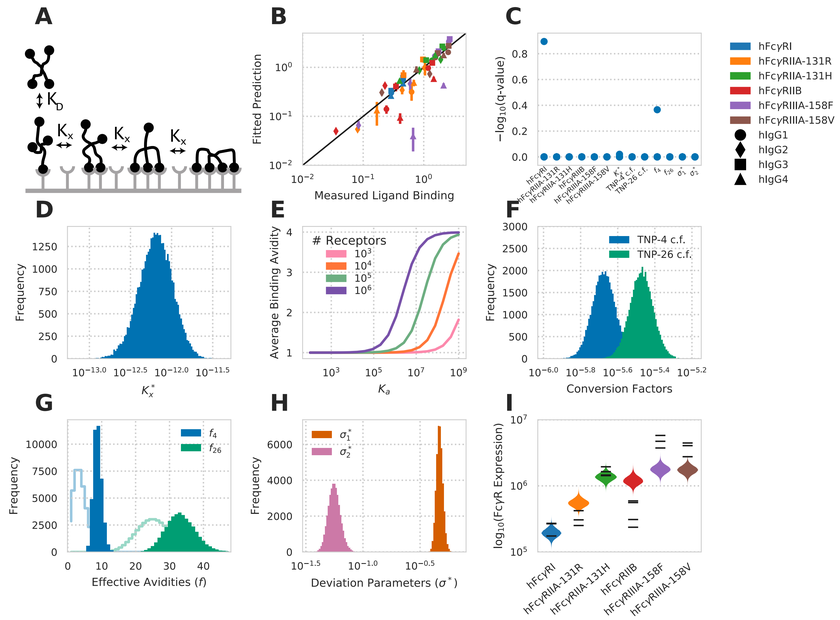

Figure 2: A multivalent binding model accounts for IgG-FcγR binding. **A)** Schematic of the multivalent binding model for interaction of an IC with a single species of hFcγR. **B)** Predicted versus measured binding for each hFcγR-hIgG pair at each valency. **C)** Geweke convergence criterion for each walker of the MCMC chain. A significant p-value would indicate failed convergence. **D)** Marginal distribution for the crosslinking constant . **E)** Average binding valency predicted for a single interaction between a cell and an IC of valency four, versus monovalent binding affinity at varied receptor expression levels. **F)** Marginal distribution for the constants to convert IC binding to normalized MFI. **G)** Marginal distribution for the effective valencies of TNP-4-BSA and TNP-26-BSA. Prior shown as line. **H)** Marginal distribution for each distribution spread parameter. **I)** The marginal distributions for receptor expression within each cell line expressing a single hFcγR subtype. Experimental measurements of receptor expression (Fig. 1B) are individually overlaid.

A binding model provides specific predictions for the coordinate effects of IC abundance, valency, and IgG subclass

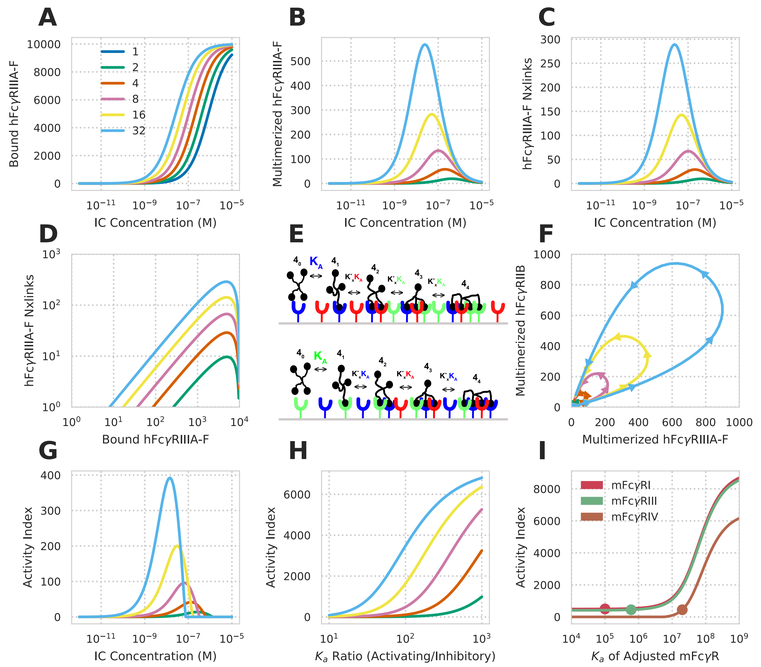

Figure 3: Specific predictions for the coordinate effects of IC parameters. **A-C)** Predicted hFcγRIIIA-F-hIgG1 binding (A), multimerized receptor (B), and number of receptor crosslinks (C) versus IC concentration at varied valencies (colors). **D)** The amount of receptor bound versus number of crosslinks for varied valency. **E)** Schematic of the multivalent binding model for interaction of an IC with multiple species of FcγR. An individual IC can interact with a heterogeneous mix of receptors according to their affinities. The effective association constant for any crosslinking step is proportional to affinity. **F)** The predicted amount of multimerized receptor at various valencies for a cell expressing hFcγRIIIA-F and hFcγRIIB simultaneously when hIgG1-IC concentration is varied from 1 pM to 10 μM (beginning and ending near the origin). **G)** The calculated activity index (see Methods) for the conditions in F. **H)** Change in the activity index versus the A/I ratio for variations in hFcγRIIIA-F affinity responding to 1 nM hIgG1-ICs. **I)** Change in the activity index upon varying the affinity of mFcγRI, mFcγRIII, and mFcγRIV simultaneously expressed along with mFcγRIIB responding to 1 nM mIgG2b-ICs at a valency of 5. Dot indicates the affinity of the receptor when not varied. Activity index increased by 50 at all values of for mFcγRI to make its curve visible.

An IgG-FcγR binding model deconvolves *in vivo* function

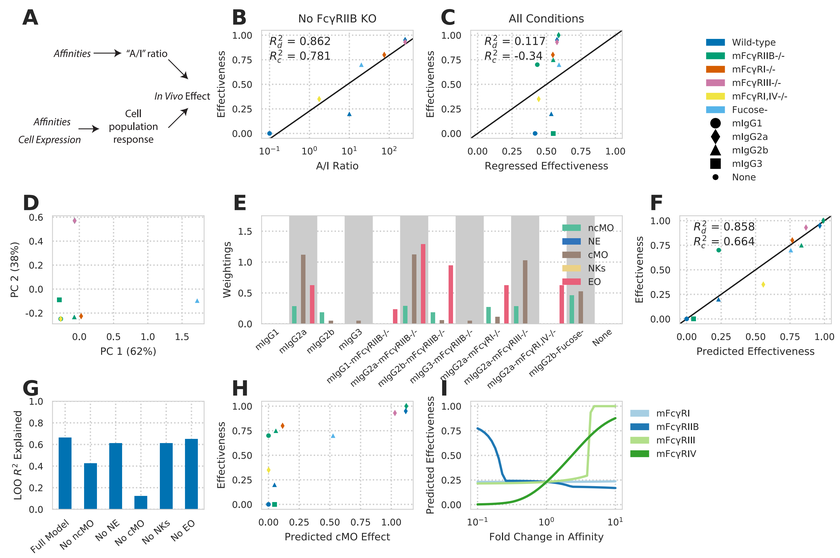

Figure 4: An FcγR-IgG binding model deconvolves in vivo function. **A)** Schematic of earlier IgG subclass experiments (top) and our approach (bottom). **B)** Effectiveness (proportional reduction in lung metastases) of individual mIgG interventions versus the A/I ratio for each mIgG constant region. Effectiveness is the fractional reduction in lung metastases observed with treatment throughout (e.g. no reduction is 0.0, while a full reduction in metastases is 1.0). **C)** Predicted versus regressed effectiveness for mIgG interventions upon mFcγR knockout using the maximal activating mFcγR affinity and inhibitory mFcγR affinity. **D)** Principal components analysis of the relevant affinities within each condition of mIgG treatment along with mFcγR knockout. Both axes scaled by a factor of 10. **E)** Individual quantities calculated for each intervention using receptor multimerization predicted by multivalent binding model and the activity index. Each quantity is scaled according to the weighting applied by the fitted regression model. **F)** Effectiveness predicted by the multivalent binding model, quantified by activity index, versus observed effectiveness. **G)** Leave-one-out model prediction R with individual input components removed. **H)** Calculated activity index for cMO versus overall effectiveness of each intervention. **I)** Predicted effect of modulating each individual mFcγR affinity of mIgG2b.

Conclusion

- Avidity most prominently modulates low-affinity FcγR-immune complex binding
- A multivalent binding model can quantitatively predict FcγR-immune complex binding
- Immune complex valency has an outsized contribution to FcγR multimerization as compared to binding
- A binding model deconvoles and predicts the influence of interventions modulating *in vivo* FcγR-driven effector function

Future directions

- Extending our model of binding to ICs of mixed IgG class
- Mapping effector function for murine and human IgGs and FcγRs
- Identifying cases of synergistic effector function when multiple IgG classes are present
- Globally mapping the effects of IC composition on effector response across different effector cell populations

Acknowledgements

This work was supported by NIH DP5-OD019815 to A.S.M., a Terri Brodeur Breast Cancer Foundation Fellowship to A.S.M., DFG-CRC1181-A07 to F.N., DFG-TRR130-P13 to F.N., and in part by the UCLA Jonsson Comprehensive Cancer Center (JCCC) grant NIH P30-CA016042. The authors wish to thank Song Yi Bae, Simin Manole, and Ted Richards for helpful feedback.

UCLA Samueli School of Engineering